

## Improving ORR Activity of Nitrogen-Doped Carbon Catalysts via Washing PANI-iron Coordination Precursor with ethanol

Yuzhen Zhang<sup>1</sup>, Jiangying Yu<sup>1</sup>, Changwei Shao<sup>1</sup>, Peichuan Sun<sup>1</sup>, Chungang Min<sup>1,2</sup>, Jianhua Wang<sup>1,2</sup>, Xikun Yang<sup>1,2,\*</sup>

<sup>1</sup> School of Materials Science and Engineering, Kunming University of Science and Technology, Kunming 650093, China

<sup>2</sup> Research Center for Analysis and Measurement, Kunming University of Science and Technology, Kunming 650093, China

\*E-mail: [yxk630@hotmail.com](mailto:yxk630@hotmail.com)

Received: 8 October 2018 / Accepted: 11 December 2018 / Published: 7 February 2019

---

Effectively improving catalytic activity of nitrogen (N)-doped carbon catalysts in oxygen reduction reaction (ORR) is very important but still facing with challenges. Herein, we proposed a “solvent effect” strategy to prepare a high active N-doped carbon catalyst with trace iron (N-C-Fe-ethanol, 0.10 at.% Fe) via pyrolysis of polyaniline (PANI)-iron (Fe) coordination polymer washed with ethanol. Electrochemical results show that N-C-Fe-ethanol catalyst exhibits a remarkable 109 mV positive shift of half-wave potential compared with that of catalyst unwashed PANI-Fe coordination polymer, and its limiting current density ( $3.61 \text{ mA}\cdot\text{cm}^{-2}$ ) is closer to that of Pt/C catalyst in acid media. It was demonstrated that the surface structure of PANI-Fe coordination polymer could be tuned via removing some nitrogen-containing groups such as  $-\text{N}^+=$  groups and other small molecules on its surface, which helped to generate a high ratio of graphitic N in the pyrolysis process. This work develops a new path for improving the ORR activity of N-doped carbon catalysts.

---

**Keywords:** Nitrogen-doped carbon catalyst; solvent effect; ethanol; ORR activity

### 1. INTRODUCTION

ORR is the most important reaction in clean renewable energy conversion systems such as fuel cells and metal-air batteries [1-5]. As platinum is mostly needed at the cathode owing to slow ORR kinetics [6], it is urgent to search low-cost non-precious-metal catalysts (NPMCs) for alternatives to the high-cost Pt catalysts to catalyze this reaction. Among various NPMCs, N-doped carbon catalyst is also the most promising candidate because of its high ORR activity [7-12]. Especially in recent years, the ORR activities of N-doped carbon catalysts with trace iron were almost as same as those of Fe-N-C

catalysts [13-15]. For instance, our team [16] prepared a high active N/C/Fe-c catalyst with trace iron toward the ORR due to homogenous distribution of Fe in the precursor by coordination between Fe<sup>3+</sup> and PANI. However, it is still difficult to gain high activity and stability for these catalysts, which can be comparable with Pt catalysts in acid condition.

To explore ways of enhancing ORR activities of N-doped carbon catalysts, much research work has been done till now. For example, Ding [17] reported that ORR activity of nitrogen-doped graphene was improved by space-confinement-induced synthesis. Subsequently, they [18] developed a shape fixing approach via salt recrystallization to efficiently synthesize a highly active N-doped carbon catalyst for ORR. Ferrero [19] prepared Fe-N-doped carbon capsules with outstanding performance and stability for the ORR activity in both acid and alkaline conditions via enriching Fe-N coordination sites. Jiang [20] developed a new highly active N-C-Fe ORR catalyst via Fe/Fe<sub>3</sub>C nanocrystals boosting the activity of Fe-N<sub>x</sub> coordination sites. Although the ORR activities of these catalysts had been greatly improved, their preparation technique required complex synthetic processes.

Recently, PANI was widely used as nitrogen-containing precursor to prepare a high active N-doped carbon catalyst for ORR [21-23] due to its advantages of low cost, high conductivity, good stability, and unique redox reaction characteristics [24]. However, we all know that there are three states (N<sub>1</sub>, N<sub>2</sub>, N<sub>3</sub>) of nitrogen in protonic acid doped PANI, which are attributed to the -NH- groups, the -N<sup>+</sup>H- groups and -N<sup>+</sup>= groups, respectively [25, 26]. Some oligomers and small molecules [27] are also produced during the polymerization of aniline. Unfortunately, those previous works were not taken into account that the three nitrogen-containing group structures and unstable oligomers in PANI could affected the structure of ORR active sites during pyrolysis, which could have a great impact on the catalytic performance of the N-doped carbon catalysts.

To address this problem, we proposed a “solvent effect” strategy to remove unstable components of PANI-Fe coordination polymer according to the Like-Dissolves-Like Rule [28]. The N-doped carbon catalyst with trace iron (N-C-Fe-ethanol, 0.10 at.% Fe) was prepared via pyrolysis of PANI-Fe coordination polymer washed with ethanol. The obtained catalyst exhibits a significantly enhanced catalytic activity for ORR due to the elimination of the -N<sup>+</sup>= groups and some other small molecules after washing PANI-Fe coordination polymer with ethanol.

## 2. MATERIALS AND METHODS

### 2.1 Materials

Aniline, Ammonium iron(III) sulfate (H<sub>4</sub>FeNO<sub>8</sub>S<sub>2</sub>·12H<sub>2</sub>O) and ammonium persulphate ((NH<sub>4</sub>)<sub>2</sub>S<sub>2</sub>O<sub>8</sub>) were purchased from Aladdin Co. Ltd (AR grade, shanghai, China). Sulfuric acid (AR grade) come from Chongqing Chuandong Chemical Co., Ltd. (Chongqing, China). Ethanol was supplied from Tianjin Sailboat Chemical Reagent Technology Co., Ltd. (AR grade, Tianjin, China).

### 2.2 Synthesis of catalysts

Synthesis of PANI-Fe-unwashed and PANI-Fe-ethanol: The PANI-Fe coordination polymer was

synthesized by chemical oxidation and ammonium persulphate was used as an oxidant [29]. The molar ratio of aniline to transition metal salt was 8:1. Firstly, 400 mL of a 1 mol/L sulfuric acid solution was added with  $\text{H}_4\text{FeNO}_8\text{S}_2 \cdot 12\text{H}_2\text{O}$ , stirred until completely dissolved, and 20 mL of aniline was added to completely form A solution. 9.265 g of ammonium persulphate was added to 100 mL of 1 mol/L sulfuric acid solution, and stirred until completely dissolved to form a B solution. The solution B was added to the solution A drop by drop, stirred at a temperature of 5 °C for 30 min to form a dark green mixture, then continued to react at 24 °C for 24 h to obtain a suspension. The suspension was then filtered with suction to obtain a filter cake. Then the cake was divided into two parts. One part was kept in the original synthetic state without solvent cleaning named PANI-Fe-unwashed, while the other part was soaked in anhydrous ethanol for 15 minutes and then filtered named PANI-Fe-ethanol. These two cakes were drying under vacuum at 60 °C for 12 hours and grinding with agate.

Synthesis of N-C-Fe-unwashed and N-C-Fe-ethanol: PANI-Fe-unwashed and PANI-Fe-ethanol were respectively obtained as a nitrogen source and a carbon source precursor. These two precursor powders were heat-treated at 900 °C for 1h in  $\text{N}_2$  atmosphere to obtain N-C-Fe-unwashed and N-C-Fe-ethanol catalysts, respectively.

### 2.3 Physical and electrochemical characterization

Scanning electron microscopic (SEM) observation was conducted on a Nova Nano 450 to analyze the morphology of the PANI-Fe coordination polymer. Transmission electron microscopic (TEM) measurement was conducted on a Tecnai G<sup>2</sup> TF30 S-Twin equipped with an EDS detector at an acceleration voltage of 100 kV to observe the microstructure of the PANI-Fe coordination polymer and N-doped carbon catalyst. TEM samples were prepared by drop casting a catalyst dispersion directly onto a copper grid coated with a holey carbon film. Then we used Fourier transform infrared spectroscopy (FT-IR, AVATAR 360 FT-IR), Raman Spectra (Raman, Uv-Vis Raman System 1000), X-ray Photoelectron Spectrometer (XPS, PHI5000 Versa Probe II) and X-ray Diffractometer (XRD, Rigaku D/max-220) to carefully analyze the chemical composition, chemical state, and chemical structure of PANI-Fe coordination polymer and N-doped carbon catalyst.

Cyclic voltammetry and linear sweep curves were measured at room temperature using 0.5 mol/L  $\text{H}_2\text{SO}_4$  solution as the electrolyte and a standard three-electrode system. The platinum plate and the Ag/AgCl electrode (3.5 M solution of KCl in the reference solution) were the counter electrode and the working electrode, respectively. A catalyst-loaded glassy carbon electrode (GC, diameter 4 mm) was used as a working electrode. Firstly, a mixture of 950  $\mu\text{L}$  of isopropanol and 50  $\mu\text{L}$  of 5% Nafion was added to 6 mg catalyst, and sonicated in an ice bath (over 30 min) until the mixed solution became a uniform ink-like slurry. Pipetted 10  $\mu\text{L}$  of the slurry dropwise on the GC surface, then placed the electrode on a digital infrared lamp at 40 °C for 20 minutes. The loading of the GC surface catalyst was about 480  $\mu\text{g} \cdot \text{cm}^{-2}$ . For comparison, we tested a commercial Pt/C (20 wt.% Pt, Johnson-Matthey) catalyst under the same test conditions. The electrochemical potentials of all the test data in this paper were converted to potentials relative to the potential of RHE.

### 3. RESULTS AND DISCUSSION

#### 3.1 Morphological and structural characterization

The SEM images of PANI-Fe-unwashed and PANI-Fe-ethanol precursors are shown in Figure 1, A and B. It can be seen that both of them are composed of granular aggregates about 100 nm ~ 50 $\mu$ m in size. However, some messy linear polymers are distributed incoherently in Figure 1A. Interestingly, they completely disappeared after being washed with ethanol in Figure 1B.

TEM was employed to investigate to further discern the microstructure of PANI-Fe-unwashed and PANI-Fe-ethanol precursors. Figure 1C shows that each aggregate is made of flake particles, while the aggregate consisted of serrated particles is observed in Figure 1D. This result shows that morphology of the PANI particles has changed dramatically after being washed with ethanol.

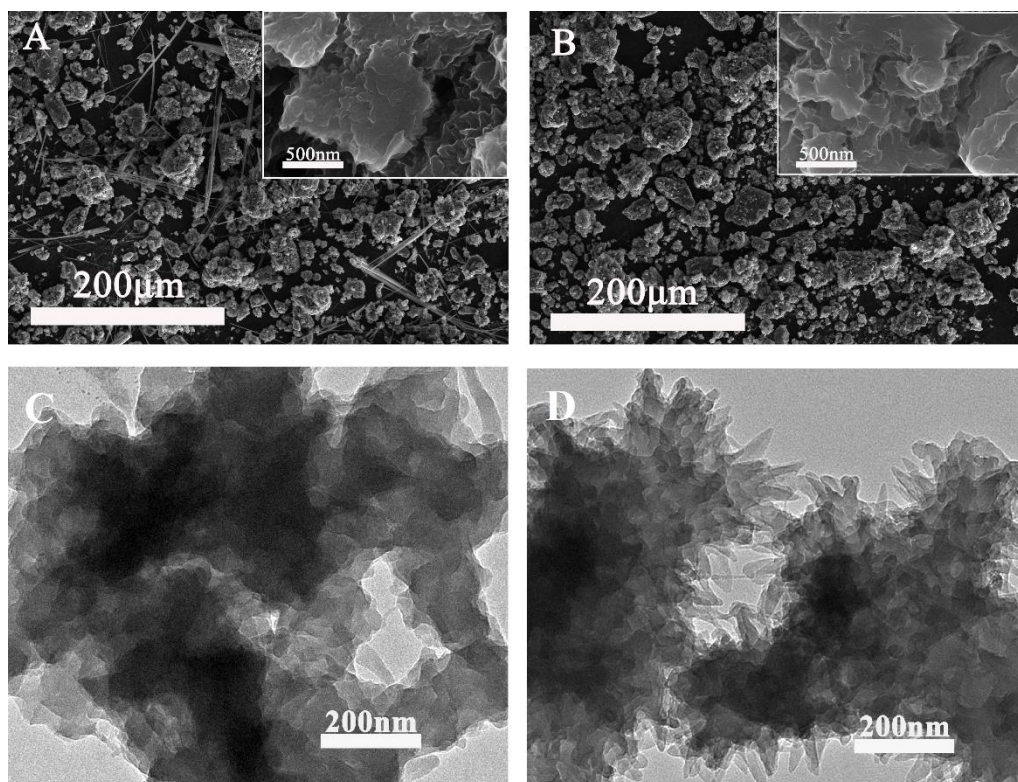


**Figure 1.** SEM images of PANI-Fe-unwashed (A), PANI-Fe-ethanol (B), TEM images of PANI-Fe-unwashed (C), PANI-Fe-ethanol (D)

The infrared spectra of PANI-Fe-unwashed and PANI-Fe-ethanol precursors are shown in Figure 2. The broad peak of PANI-Fe-unwashed at 3435  $\text{cm}^{-1}$  is the stretching vibration of  $-\text{NH}_2$  [30], while the absorption peaks at 2932  $\text{cm}^{-1}$  and 2866  $\text{cm}^{-1}$  are intramolecular and intermolecular hydrogen bonding N-H stretching vibrations or frequency bands on secondary amines [31]. The absorption peaks at 1222  $\text{cm}^{-1}$  and 1125  $\text{cm}^{-1}$  are the  $\text{C}-\text{N}^+$  stretching vibration mode and the  $\text{B}-\text{NH}^+=$  vibration mode [32], respectively. And the absorption peaks at 1175  $\text{cm}^{-1}$ , 1059  $\text{cm}^{-1}$ , 1222  $\text{cm}^{-1}$  and 588  $\text{cm}^{-1}$  are assigned to the  $\nu_3$  mode of  $\text{SO}_4$  [33] and the sulfuric acid counter ion (symmetric  $\text{SO}_3$  stretching vibration) [34]. It

can be seen that the intensity of these peaks in the PANI-Fe-ethanol spectra is significantly weaker than those in the PANI-Fe-unwashed, which indicates that the oligomer and some other organic small molecules were removed by washing with ethanol. The XRD patterns of PANI-Fe-unwashed and PANI-Fe-ethanol precursors are shown in figure S2, which exhibit typical PANI diffraction peaks [35] (Supplementary 2, fig. S2).

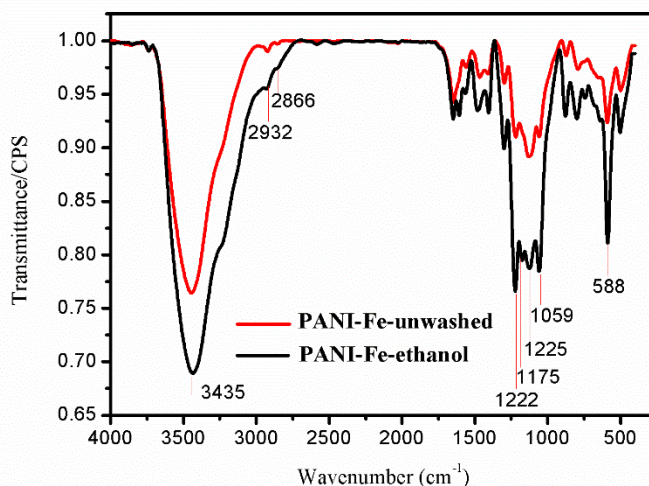


**Figure 2.** FTIR spectra of PANI-Fe-unwashed and PANI-Fe-ethanol

Low-resolution TEM images of N-C-Fe-unwashed and N-C-Fe-ethanol catalysts were shown in Figure 3 A, B. It can be seen that both of them are also composed of carbon particles about 20 nm ~ 1 $\mu$ m in size. The high-resolution TEM (HRTEM) images of these carbon particles exhibit the nature of amorphous carbon (inset of Figure 3, A and B). In addition, some dark spots can be observed on the amorphous carbon. However, the lattice fringes of these dark spots can not be found by HRTEM (inset of Figure 3, A and B), implying that the dark spots may be the piling of carbon particles.

To better understand the microstructure of these two amorphous carbon catalysts, we used Raman spectroscopy to analyze the defects and the degree of ordering of the carbon. The graphitic D and G bands can be clearly seen at 1350 and 1570  $\text{cm}^{-1}$ , respectively (Figure 4A). The D/G band intensity ratio of N-C-Fe-ethanol ( $I_D/I_G=1.156$ ) is larger than that of N-C-Fe-unwashed ( $I_D/I_G=1.007$ ), indicating that the N-C-Fe-ethanol catalysts have more defects and disorder compared with N-C-Fe-unwashed catalysts.

Figure 4B is XRD pattern of the N-C-Fe-unwashed and N-C-Fe-ethanol catalysts, which show peaks at 24.8°, 35.6°, 43.4°, 44.5° and 81.8°, respectively. The diffuse broad peaks at 24.8° and 43.4° are attributed to the (002) crystal plane of graphite carbon and (110) crystal plane [36, 37]. The peak at 35.6° corresponds to the (200) crystal plane of  $\text{Fe}_2\text{O}_3$  [38]. The diffraction peak at 44.5° and a protrusion near 81.8° exposed in N-C-Fe-ethanol catalyst, which is a characteristic peak of the (211) and (322) crystal planes of  $\text{Fe}_7\text{C}_3$  (PDF card: 17-0333). This indicates that the two catalysts are mainly composed of disordered carbon small amounts of  $\text{Fe}_2\text{O}_3$  and  $\text{Fe}_7\text{C}_3$ . However, the amount of  $\text{Fe}_7\text{C}_3$  in N-C-Fe-ethanol catalyst is reduced obviously by being washed with ethanol.

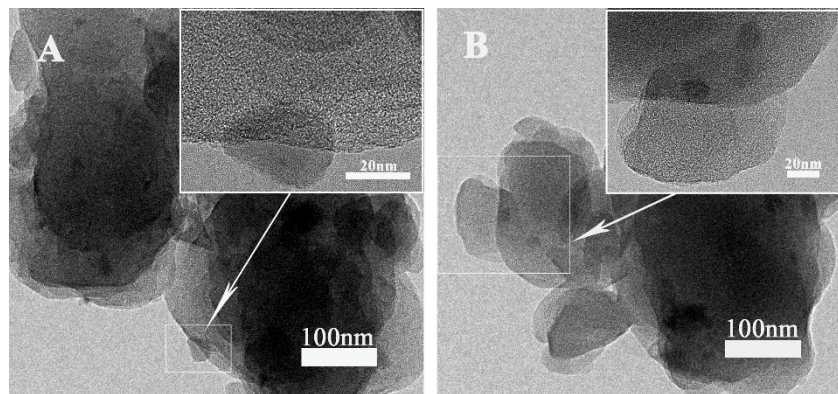


**Figure 3.** TEM images of N-C-Fe-unwashed (A), N-C-Fe-ethanol (B)

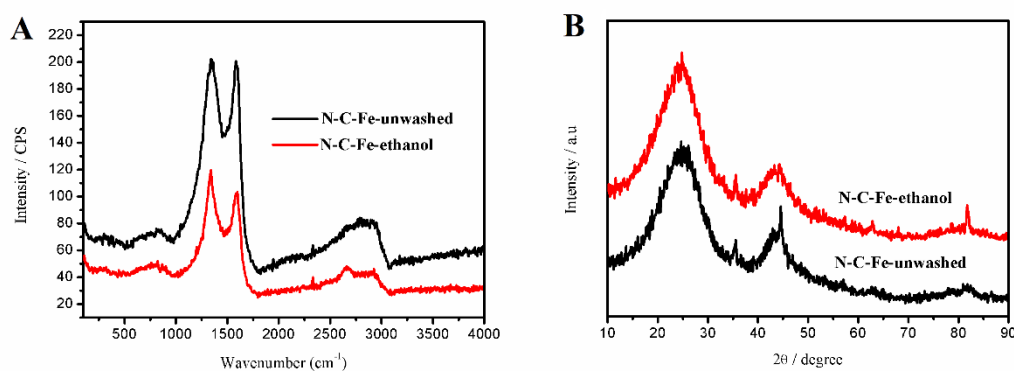


**Figure 4.** Raman spectra of N-C-Fe-unwashed and N-C-Fe-ethanol (A), XRD patterns of N-C-Fe-unwashed and N-C-Fe-ethanol (B)

### 3.2 Electrochemical characterization

Figure 5A are CV curves of the N-C-Fe-unwashed and the N-C-Fe-ethanol catalysts in  $N_2$  saturated 0.5 M  $H_2SO_4$  solution after the 50th cycles. It can be seen that their CV curves show a pair of redox peaks at the potential about 0.65V, which can be attributed to the  $Fe^{3+}/Fe^{2+}$  redox couple. However, the area of CV curve for N-C-Fe-ethanol catalyst is obviously larger than that of CV curve for N-C-Fe-unwashed catalyst, which indicates that the mass specific capacitance of the former is larger than the latter. The LSV curves of N-C-Fe-unwashed, N-C-Fe-ethanol catalyst and commercial Pt/C catalyst (20 % JM) are presented in Figure 5B.

The initial reduction potential, half-wave potential and limiting current density of the N-C-Fe-ethanol catalyst are 0.78 V, 0.656 V and  $3.61 \text{ mA}\cdot\text{cm}^{-2}$ , respectively, while these of N-C-Fe-unwashed catalyst are 0.75 V, 0.547 V and  $2.92 \text{ mA}\cdot\text{cm}^{-2}$  (table 1). The half-wave potential of N-C-Fe-ethanol catalyst, which is higher than that reported by literature [14] and [19], is 109 mV higher than that of N-C-Fe-unwashed catalyst, the initial reduction potential is increased by 37mV, and the limiting current density is increased by  $0.69 \text{ mA}\cdot\text{cm}^{-2}$ . The limiting current density of the N-C-Fe-ethanol catalyst is closer to the limiting current density of the 20% Pt/C catalyst. These indicate that the ORR activity of the N-C-Fe-ethanol catalyst is greatly improved due to washing with ethanol. The kinetic analysis of ORR at the N-C-Fe-unwashed and N-C-Fe-ethanol catalysts were investigated using the rotating disk

electrode in O<sub>2</sub> saturated 0.5 M H<sub>2</sub>SO<sub>4</sub> solution from 900 rpm to 2700 rpm (See Figure 2, C and D). The insets in Figures 5, C and D are Koutecky-Levich slope plots for different N-C-Fe-unwashed and N-C-Fe-ethanol catalysts at different potentials. According to the Koutecky–Levich equations, the average number of electron transfer of N-C-Fe-unwashed and N-C-Fe-ethanol catalysts are 3.85 and 4.2 respectively, indicating that the ORR process for both catalysts is a four electron pathway.

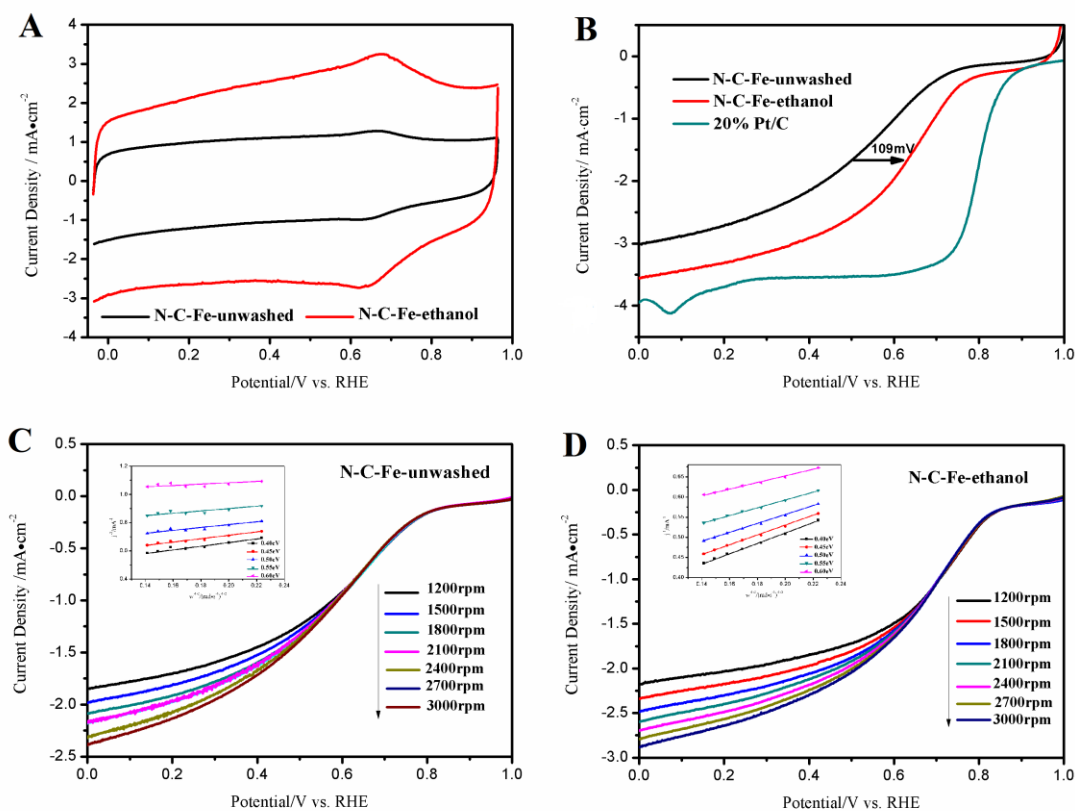


**Figure 5.** CVs recorded for N-C-Fe-unwashed and N-C-Fe-ethanol catalysts in N<sub>2</sub>-saturated 0.5 M H<sub>2</sub>SO<sub>4</sub> solution (A); LSVs at 1500 rpm for N-C-Fe-unwashed) and N-C-Fe-ethanol catalysts along with commercial 20 wt.% Pt/C catalyst in O<sub>2</sub>-saturated 0.5 M H<sub>2</sub>SO<sub>4</sub> solution (B). LSVs of N-C-Fe-unwashed (C) and N-C-Fe-ethanol (D) in O<sub>2</sub>-saturated 0.5 M H<sub>2</sub>SO<sub>4</sub> solution at various rotation speeds. Inset is the corresponding Koutecky-Levich plots.

**Table 1** The initial reduction potential, half-wave potential and limiting current density of the literature, 20% Pt/C, N-C-Fe-unwashed and N-C-Fe-ethanol catalyst.

	Initial reduction potential / V	Half-wave potential / V	Limiting current density /mA · cm <sup>-2</sup>
Literature [14]	0.80	0.592	4.95
Literature [19]	0.80	0.520	3.52
20% Pt/C	0.85	0.805	2.55
N-C-Fe-unwashed	0.75	0.547	2.92
N-C-Fe-ethanol	0.78	0.656	3.61

### 3.3 Surface chemical composition and structure analysis

In order to gain further insight into origin of improving ORR activity, XPS was used to analyze the surface chemical composition and structure of PANI-Fe-unwashed, PANI-Fe-ethanol, N-C-Fe-unwashed and the N-C-Fe-ethanol. The XPS survey spectra of PANI-Fe-ethanol and PANI-Fe-unwashed show the presence of C, O, N and S, respectively (figure S3), and their atomic concentration are shown in Table S1. It can be seen from Table S1 that the atomic concentrations of O and S in the PANI-Fe-ethanol are reduced compared with that in the PANI-Fe-unwashed. XPS fit results of N1s of PANI-Fe-unwashed and PANI-Fe-ethanol are shown in Figure 6, A and B and Table S2. The N1s spectra were analyzed by least-squares fitting analysis, which includes the components of the phenylenediamine ( $N_1$ : -NH-) structure ( $399.5 \pm 0.4$  eV), the amino group ( $N_2$ :  $-N^+H-$ ) nitrogen structure ( $400.8 \pm 0.4$  eV), and the protonated imine ( $N_3$ :  $-N^{+}=$ ) structure ( $402.2 \pm 0.4$  eV) [16,26,39]. It can be seen from Figure 6, A and B that some  $-N^{+}=$  groups has been removed after being washed with ethanol, indicating that surface chemical structure of the PANI-Fe-ethanol has changed after washing with ethanol.

As an important parameter to evaluate the degree of polyaniline doping, the  $R_{[N^+]/[N]}$  of the PANI-Fe-unwashed and PANI-Fe-ethanol precursors are calculated. The value of PANI-Fe-ethanol is close to the ideal ectopic polyaniline doped value of 0.5 (Table S2), revealing that dedoping of  $H^+$  occurs after the surface of the sample is cleaned with ethanol. This result is consistent with that the O and S atoms ( $SO_3^{2-}$ ,  $SO_4^{2-}$ ) decreased after washing with ethanol in XPS and infrared test results.

The XPS survey spectra of N-C-Fe-unwashed and N-C-Fe-ethanol catalysts show the presence of C, O, N, S and trace Fe, respectively (figure S4), and their atomic concentrations are shown in Table S3. It can be seen from Table S2 that the atomic concentrations of O, S, and Fe in the N-C-Fe-ethanol are almost same as that of O, S, and Fe in the N-C-Fe-unwashed.

The N1s XPS spectra of N-C-Fe-unwashed catalyst can be divided into four peaks: pyridinic nitrogen (398.5 eV, 30.1%), pyrrolic nitrogen (400.1 eV, 30.1%), graphitic nitrogen (401.1 eV, 34.8%) and oxide nitrogen (403.2 eV, 5.0%) [20,40,41], while that of N-C-Fe-ethanol catalyst can only be divided into three peaks (Figure 6B): pyridinic nitrogen (398.5 eV, 8.7%), pyrrolic nitrogen (400.1 eV, 42.2%) and graphitic nitrogen (401.1 eV, 49.1%). By comparison, it can be found that the N-C-Fe-ethanol catalyst contains a higher proportion of graphitic N than the N-C-Fe-unwashed catalyst, while its pyridinium N is decrease and oxide N disappears.

Based on the above analysis, we find that the binding energy of pyridinium N, pyrrole N and graphite N are close to that of the three nitrogen-containing group peaks ( $N_1$ ,  $N_2$ ,  $N_3$ ) respectively (Figure 6A and B), suggesting that they have similar chemical environment. Meanwhile, this result imply that the change of three nitrogen-containing groups in PANI can affect the active site structure of N-doped carbon catalyst during pyrolysis, which will further have a great impact on its catalytic performance.

Combined with the result of electrochemical characterization, we demonstrate that the  $-N^{+}=$  groups and some other small molecules (oligomers, sulfate and etc.) in the PANI-Fe coordination polymer were largely eliminated after washing with ethanol, and enhanced ORR activity of the N-C-Fe-ethanol catalyst can be ascribed to the elimination of the  $-N^{+}=$  groups and some other small molecules, which helps to generate a high ratio of graphite N in the pyrolysis process.

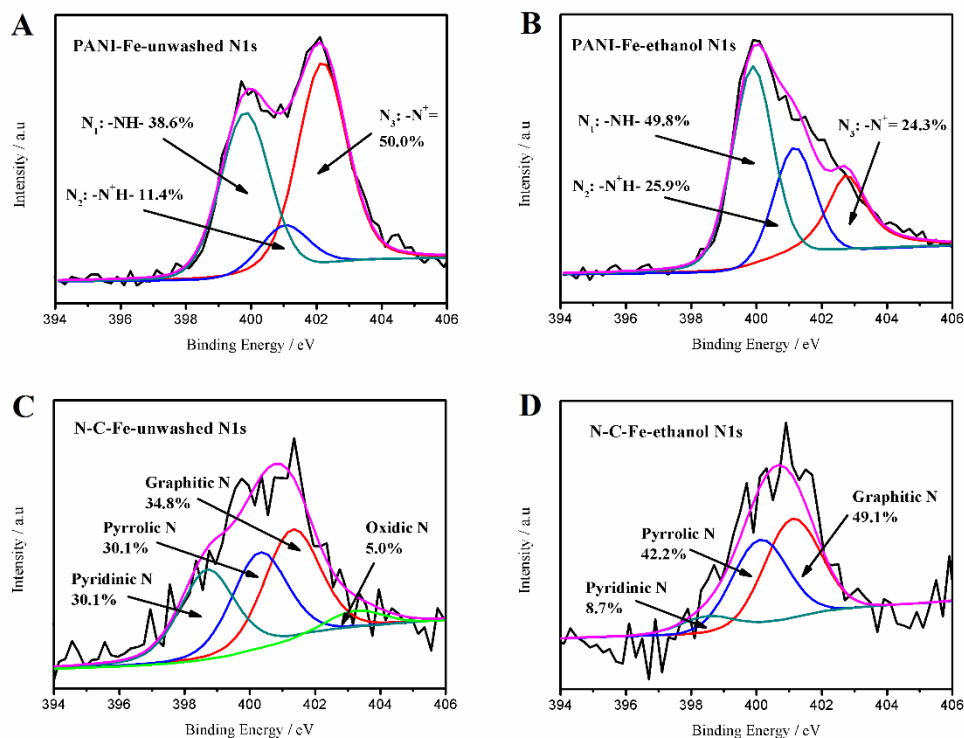


**Figure 6.** The XPS fitting spectra of N1s region for PANI-Fe-unwashed (A); PANI-Fe-ethanol (B); N-C-Fe-unwashed(C) and N-C-Fe-ethanol (D).

#### 4. CONCLUSION

In summary, we have successfully synthesized a high active N-C-Fe catalyst derived from an aniline-iron coordination polymer washed with ethanol. The morphology of the PANI polymer particles has changed dramatically after being washed with ethanol. More importantly, it is found that the change of nitrogen-containing groups in PANI lead to the ratio alteration of N sites after pyrolysis, which will further have a great significance on improving catalytic performance of N-doped carbon catalyst. The improvement of ORR activity is due to the increase of the proportion of graphitic nitrogen. This finding provided ideas for the development of nitrogen-doped carbon-based catalysts.

#### SUPPLEMENTARY MATERIAL:

##### 1. SEM Images of PANI-Fe Precursors

The SEM images of PANI-Fe-unwashed and PANI-Fe-ethanol precursors are shown in figure S1. It is obvious that the messy linear molecules disappeared in PANI-Fe-ethanol, which are distributed incoherently in PANI-Fe-unwashed.

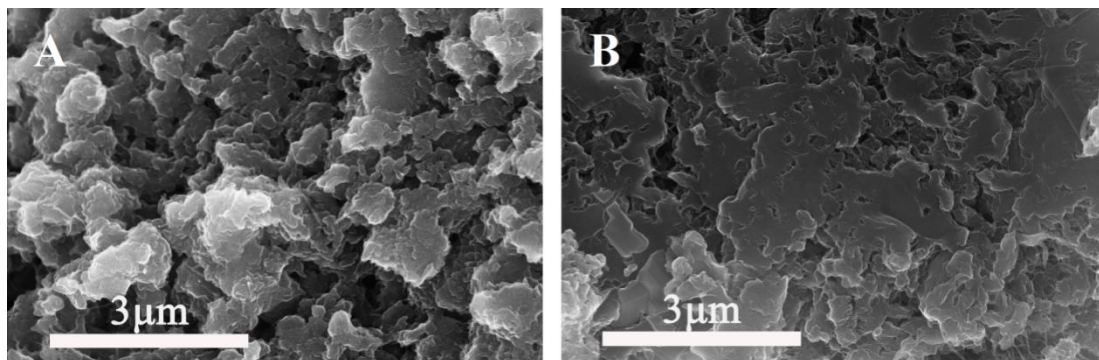


**Figure. S1** SEM images of PANI-Fe-unwashed (A) , PANI-Fe- ethanol (B)

## 2. XRD Characterization of PANI-Fe Precursors

Figure S2 shows the XRD patterns of PANI-Fe-unwashed and PANI-Fe-ethanol precursors. The PANI-Fe-ethanol exhibited significant diffraction peaks at  $2\theta$  of  $20.5^\circ$  and  $25.2^\circ$ , and a shoulder protruded near  $26.7^\circ$ , corresponding to peaks at  $21^\circ$ ,  $24.9^\circ$ , and  $27.4^\circ$  in PANI-Fe-unwashed, respectively. And peaks at  $15^\circ$  and  $19.5^\circ$  are a polyaniline (211) crystal plane peak and a characteristic peak of non-crystalline polyaniline. Therefore, the crystallinity of PANI-Fe-ethanol is better than that of PANI-Fe-unwashed. In addition, the peak at  $43.9^\circ$  in PANI-Fe-unwashed pattern is a carbon peak corresponding to the PDF card numbered 06-0675.

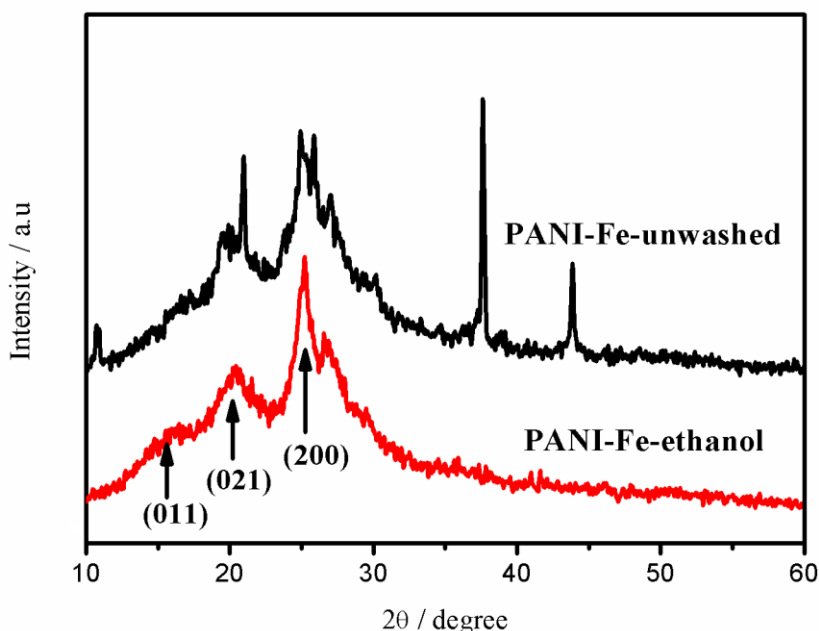


**Figure. S2** XRD patterns of PANI-Fe-unwashed and PANI-Fe-ethanol

## 3. Figures and Tables of PANI-Fe Precursors and N-C-Fe catalysts XPS analysis

Figure S3 shows the XPS survey spectra of PANI-Fe-unwashed and PANI-Fe-ethanol catalysts. Table S1 shows the surface elemental analysis of PANI-Fe-unwashed and PANI-Fe-ethanol. It can be seen that the content of O and S in the PANI-Fe-ethanol precursor is lower than that of the PANI-Fe-unwashed precursor, while the ratio of N/C is increased. This indicates that the small molecules was removed by washing with ethanol in polyaniline system with nitrogen atoms reserved.

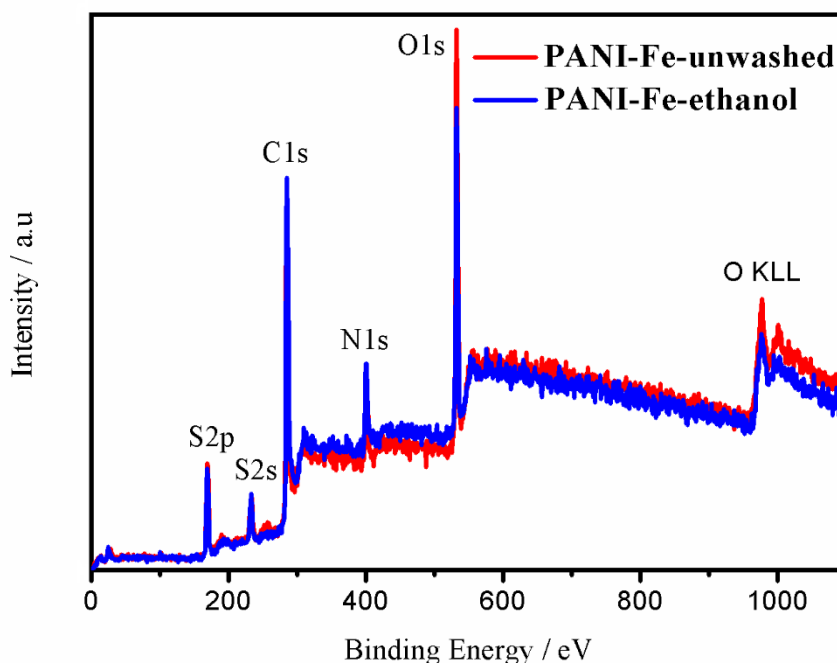


**Figure. S3** XPS survey spectra of PANI-Fe-unwashed and PANI-Fe-ethanol

**Table. S1** presents the surface elemental analysis of PANI-Fe-unwashed and PANI-Fe-ethanol

Name	C (at.%)	N (at.%)	O (at.%)	S (at.%)	N/C
PANI-Fe-unwashed	59.8	7.7	26.6	5.9	0.13
PANI-Fe-ethanol	64.2	10.3	20.6	4.9	0.16

**Table S2** shows the XPS fitting results of PANI-Fe-unwashed and PANI-Fe-ethanol. the difference in the type and intensity of  $N^+$  peaks and the  $[N^+]/[N]$  ratio  $R_{[N^+]/[N]}$  (the sum of the intensity of N:-N=, -NH-,  $N^+$ ) are important factors for the sample.

**Table S2** The XPS fitting result of N1s region for PANI-Fe-unwash and PANI-Fe-ethanol

Name		-N=	-NH-	-N <sup>+</sup> H-	-N <sup>+</sup> =
Peak Position (eV)		399.0	399.5	400.8	402.2
PANI-Fe-unwashed	%Area	0	38.6	11.4	50.0
	$R_{[N^+]/[N]}$	61.4%			
PANI-Fe-ethanol	%Area	0	49.8	25.9	24.3
	$R_{[N^+]/[N]}$	50.2%			

**Figure S4** shows the XPS survey spectra of N-C-Fe-unwashed and N-C-Fe-ethanol catalysts. Table S3 shows the XPS results for surface elemental analysis of Fe-N-C- unwashed and Fe-N-C-ethanol catalysts. It can be seen that the contents of S and Fe in Fe-N-C-unwashed and Fe-N-C-ethanol catalysts are very small, and the N and O contents of Fe-N-C-unwashed catalyst are better than that of Fe-N-C-ethanol. The initial N/C ratio calculated from the chemical structure of polyaniline is 0.125, while the N/C ratios of Fe-N-C-unwashed and Fe-N-C-ethanol are 0.0295, 0.0236, respectively, which means that 18.9-23.6% of the N atoms remain after pyrolysis at 900 °C.

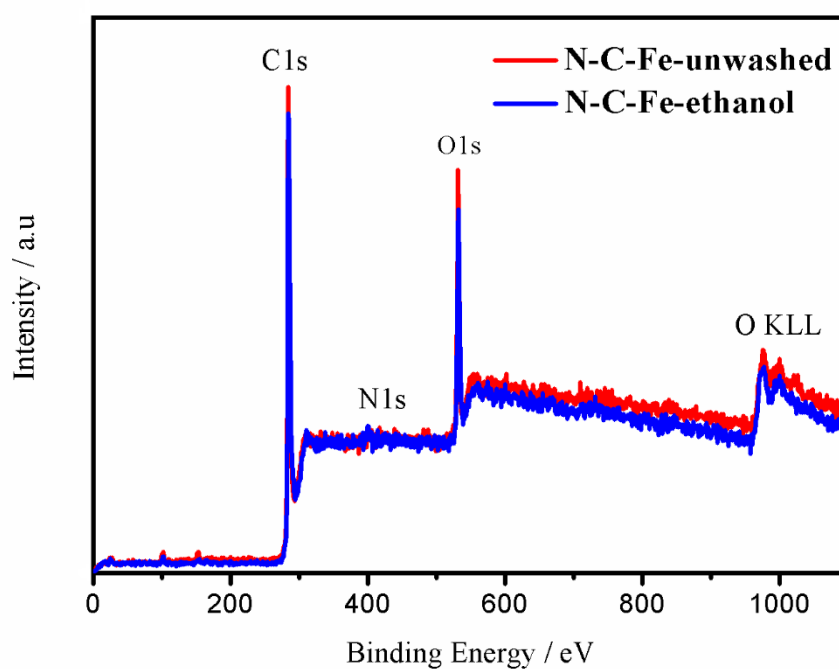


**Figure. S4** XPS survey spectra of N-C-Fe-unwashed and N-C-Fe-ethanol

**Table S3** presents the surface elemental analysis of Fe-N-C-unwashed and Fe-N-C-ethanol

Name	C (at.%)	N (at.%)	O(at.% )	S (at.%)	Fe (at.%)	N/C
N-C-Fe-unwashed	79.0	2.3	18.4	0.2	0.1	0.03
N-C-Fe-ethanol	80.0	2.7	17.2	0.0	0.1	0.03

#### ACKNOWLEDGEMENTS

This work was supported by the National Natural Science Foundation of China (Projects 11764026, 51374117, 21363012 and 51164017) and Kunming science and technology project (2015-1-G-01001).

#### References

1. E. Antolini, J. R. C. Salgado, M. J. Giz, E. R. Gonzalez, *Int. J. Hydrogen Energy*, 30 (2005) 1213.
2. S. Song, W. Yi, P. Tsiakaras, P. K. Shen, *Appl. Catal B-Environ.*, 78 (2008) 381.
3. J. Suntivich, H. A. Gasteiger, N. Yabuuchi, H. Nakanishi, J. B. Goodenough, Y. Shao-Horn, *Nat. Chem.*, 3 (2011) 647.
4. T. Takeguchi, T. Yamanaka, H. Takahashi, H. Watanabe, T. Kuroki, H. Nakanishi, Y. Orikasa, Y. Uchimoto, H. Takano, N. Ohguri, M. Matsuda, T. Murota, K. Uosaki, W. Ueda, *J. Am. Chem. Soc.*, 135 (2013) 11125.
5. H. Wang, C. Tang, B. Wang, B. Q. Li, Q. Zhang, *Adv. Mater.*, 29 (2017) 1.
6. H. A. Gasteiger, J. E. Panels, S. G. Yan, *J. Power Sources*, 127 (2004) 162.
7. K. Gong, F. Du, Z. Xia, M. Durstock, L. Dai, *Science*, 323 (2009) 760.

8. G. Wu, K. L. More, C. M. Johnston, P. Zelenay, *Science*, 332 (2011) 443.
9. S. Chen, J. Bi, Y. Zhao, L. Yang, C. Zhang, Y. Ma, Q. Wu, X. Wang, Z. Hu, *Adv. Mater.*, 24 (2012) 5646.
10. C. H. Choi, S. H. Park, S. I. Woo, *ACS Nano*, 6 (2012) 7084.
11. M. Q. Wang, W. H. Yang, H. H. Wang, C. Chen, Z. Y. Zhou, S. G. Sun, *ACS Catal.*, 4 (2014) 3928.
12. L. Lin, Q. Zhu, A. W. Xu, *J. Am. Chem. Soc.*, 136 (2014) 11027.
13. J. Chen, X. Cui, W. Zheng, *Catal. Commun.*, 60 (2015) 37.
14. Q. Wang, Z. Chen, N. Wu, B. Wang, W. He, Y. Lei, Y. Wang, *Chemelectrochem*, 4 (2017) 1.
15. X. Shi, J. Zhang, T. Huang, *J. Mater. Sci.*, 53 (2017) 1.
16. G. Wang, K. Jiang, M. Xu, C. Min, B. Ma, X. Yang, *J. Power Sources*, 266 (2014) 222.
17. W. Ding, Z. Wei, S. Chen, X. Qi, T. Yang, J. Hu, D. Wang, L. J. Wan, S. F. Alvi, L. Li, *Angew. Chem.*, 52 (2013) 11755.
18. W. Ding, L. Li, K. Xiong, Y. Wang, W. Li, Y. Nie, S. Chen, X. Qi, Z. Wei, *J. Am. Chem. Soc.*, 137 (2015) 5414.
19. G. A. Ferrero, K. Preuss, A. Marinovic, A. B. Jorge, N. Mansor, D. J. L. Brett, A. B. Fuertes, M. Sevilla, M. M. Titirici, *ACS Nano*, 10 (2016) 5922.
20. W. J. Jiang, L. Gu, L. Li, Y. Zhang, X. Zhang, L. J. Zhang, J. Q. Wang, J. S. Hu, Z. D. Wei, L. J. Wan, *J. Am. Chem. Soc.*, 138 (2016) 3570.
21. M. Ferrandon, X. Wang, A. J. Kropf, D. J. Myers, G. Wu, C. M. Johnston, P. Zelenay, *Electrochim. Acta*, 110 (2013) 282.
22. X. Wang, L. Zou, H. Fu, Y. Xiong, Z. Tao, J. Zheng, X. Li, *ACS Appl. Mater. Interfaces*, 8 (2016) 8436.
23. Shehnaz, X. Song, S. Ren, Y. Yang, Y. Guo, H. Jing, *J. Energy Chem.*, 26 (2017) 182.
24. X. Jing, L. Wang, X. Wang, Y. Gong, F. Wang, *Acta Polymerica Sinica*, 12 (2005) 655.
25. M. G. Han, S. S. Im, *Polymer*, 41 (2000) 3253.
26. L. Li, E. Liu, H. Shen, Y. Yang, Z. Huang, X. Xiang, Y. Tian, *J. Solid State Electrochem.*, 15 (2011) 175.
27. I. Sapurina, J. Stejskal, *Polym. Int.*, 57 (2008) 1295.
28. W. L. Smith, *J. Chem. Educ.*, 54 (1977) 228.
29. R. Shaimi, N. M. Ketar Mokhtar, P. C. Tan, Z. A. Jawad, S. C. Low, *e-Polym.*, 16 (2016) 225.
30. Z. Ping, *J. Chem. Soc., Faraday Trans.*, 92 (1996) 3063.
31. M. S. Ram, S. Palaniappan, *J. Mater. Sci.*, 39 (2004) 3069.
32. M. Trchová, I. Šeděnková, E. Tobolková, J. Stejskal, *Polym. Degrad. Stab.*, 86 (2004) 179.
33. M. Belhouchet, M. Bahri, J. M. Savariault, T. Mhiri, *Spectrochim. Acta. A.*, 61 (2005) 387.
34. M. Drozd, J. Baran, *Spectrochim. Acta. A.*, 64 (2006) 867.
35. H. K. Chaudhari, D. S. Kelkar, *J. Appl. Polym. Sci.*, 62 (1996) 15.
36. G. Wu, M. Nelson, S. Ma, H. Meng, G. Cui, P. K. Shen, *Carbon*, 49 (2011) 3972.
37. H. Peng, Z. Mo, S. Liao, S. Liao, H. Liang, L. Yang, F. Luo, H. Song, Y. Zhong, B. Zhang, *Sci. Rep.*, 3 (2013) 1765.
38. D. Larcher, D. Bonnin, R. Cortes, I. Rivals, L. Personnaz, *J. Electrochem. Soc.*, 150 (2003) A1643.
39. E. T. Kang, K. G. Neoh, Y. L. Woo, K. L. Tan, *Polymer*, 33 (1992) 2857.
40. Z. H. Sheng, L. Shao, J. J. Chen, W. J. Bao, F. B. Wang, X. H. Xia, *ACS nano*, 5 (2011) 4350.
41. D. Guo, R. Shibuya, C. Akiba, S. Saji, T. Kondo, J. Nakamura, *Science*, 16 (2016) 361.